On the Stiffness Matrix of the Intervertebral Joint: Application to Total Disc Replacement

Oliver M. O'Reilly, Melodie F. Metzger, Jenni M. Buckley,
David A. Moody and Jeffrey C. Lotz

Abstract

The traditional method of establishing the stiffness matrix associated with an intervertebral joint is valid only for infinitesimal rotations, whereas the rotations featured in spinal motion are often finite. In the present paper, a new formulation of this stiffness matrix is presented which is valid for finite rotations. This formulation uses Euler angles to parameterize the rotation, an associated basis, which is known as the dual Euler basis, to describe the moments, and it enables a characterization of the non-conservative nature of the joint caused by energy loss in the poroviscoelastic disc and ligamentous support structure. As an application of the formulation, the stiffness matrix of a motion segment is experimentally determined for the case of an intact intervertebral disc and compared to the matrices associated with the same segment after the insertion of a total disc replacement system. In this manner, the matrix is used to quantify the changes in the intervertebral kinetics associated with total disc replacements. As a result, this paper presents the first such characterization of the kinetics of a total disc replacement.

Index Terms

Spine kinematics, intervertebral disc, stiffness matrix, disc arthroplasty.

1 Introduction

While there are hopes of seeing vertebral disc replacement travel the same successful path as total hip and knee replacements, the complexity of the joint structure between pairs of vertebrae has caused unforeseen complications.[1] The intervertebral disc has a complex structure and function that includes synergistic functioning with the facets in constraining motion and supporting load. These structural complexities obscure optimal design choices since the relative motion of vertebra is non-trivial to characterize and measure. More importantly, inappropriate modifications to this motion may lead to other problems such as osteoarthritis in the facet joints and motion segment instability, which may lead to impingement of neural structures [5]. Spine mechanics are further complicated by a loading regime that consists of bending moments and loads that are multi-directional and often coupled.

A wide-range of measurements are currently being used to characterize spinal movements within the orthopaedic research community, including: range of motion (see, e.g., [6]), disc pressure (see, e.g., [7]), neutral zone [8], helical axis of motion (see, e.g., [9], [10]), vertebral strain (see, e.g., [11]), facet forces (see, e.g., [12], [13]), and stiffness (see, e.g., [14]). Collectively

- *O. M. O'Reilly and D. A. Moody are with the Department of Mechanical Engineering, University of California at Berkeley, Berkeley, CA 94706-1740, U.S.A.*
  E-mail: oreilly@berkeley.edu
- *Melodie F. Metzger, Jenni M. Buckley, and Jeffrey C. Lotz are with the Department of Orthopaedic Surgery, University of California at San Francisco, San Francisco, CA 94110, U.S.A.*

Manuscript submitted May 2008. Revised manuscript submitted September 2008

1. For further background on total disc replacements, see [1]–[4] and references therein.

this has provided a vast amount of information on the motion of the spine. Much of this data is crucial in the design and development of effective total disc replacements (TDR). Of particular interest in this paper is an examination of the stiffness changes induced by a TDR.

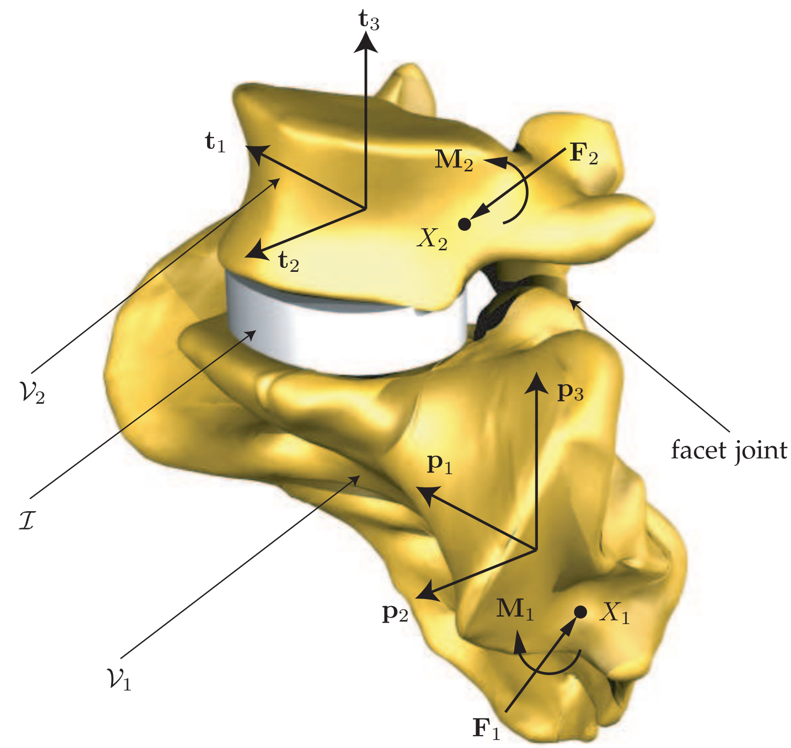

Fig. 1. *Schematic of a motion segment consisting of a pair of vertebral bodies $\mathcal{V}_1$ and $\mathcal{V}_2$ and the intervertebral disc $\mathcal{I}$. One of the pair of facet joints is also indicated, as are the bases $\{\mathbf{p}_1, \mathbf{p}_2, \mathbf{p}_3\}$ for $\mathcal{V}_1$ and $\{\mathbf{t}_1, \mathbf{t}_2, \mathbf{t}_3\}$ for $\mathcal{V}_2$. For the image shown in this figure, the lower body is S1 and the upper body is L5.*

To examine the stiffness changes induced by a TDR, one is first lead to the seminal paper by Panjabi et al. [14] which was published in 1976. In [14], a stiffness matrix characterizing a six degree-of-freedom vertebral motion segment in the thoracic spine was proposed. Using symmetry arguments, restricting attention to infinitesimal rotations, and assuming certain symmetries, the number of stiffnesses in this matrix were reduced from 36 to 12. Subsequent work by Gardner-Morse, Stokes et al. [15]–[18], have measured these 12 parameters. A related stiffness matrix for the lumbar spine was proposed by McGill and Norman [19], and in subsequent works the potential energy of the muscle forces and external forces was incorporated into this matrix (see Cholewicki and Norman [20], Howarth et al. [21], McGill and Bennett [22], and references cited therein).

Unfortunately, the stiffness matrices proposed by Panjabi et al. [14] and McGill and Norman [19] have several restrictions which limit their utility. The most problematic is the inability to accommodate finite rotations and energy losses due to the poroviscoelastic nature of the intervertebral disc and the nonconservative forces and moments due to the facet joints and ligaments. These and other deficiencies are addressed in this paper by presenting an alternative method of calculating the stiffness matrix of a motion segment. The segment in question consists of two vertebral bodies, their adjoining intervertebral disc, the facet joints, and the ligaments connecting the two bodies. The construction of the stiffness matrix is performed with the help of the developments in O'Reilly [23] and O'Reilly and Srinivasa [24], and by exploiting a recently developed basis which is known as the dual Euler basis. The methodology is valid for finite rotations and can accommodate the (non-conservative) forces and moments due to the facet joints and ligaments. Thus, the matrix proposed in this paper will be non-symmetric due to the nonconservative forces that are included in the model.

The use of the dual Euler basis in the present paper is similar to the use of a related dual basis in Howard et al. [25] and Žefran and Kumar [26] which recently came to the attention of the authors. In this pair of papers, Žefran et al. use screw theory to describe the wrench (force and moment) components with respect to a dual basis and use these components to establish a stiffness-twist relationship. Their basis couples the individual components of the twists (displacements and rotations), and their work could also be used to formulate a stiffness matrix for the motion segment.[2]

The primary aim of the present paper is to introduce the theory which supports this new formulation of the stiffness matrix. Secondly, a method for distilling the 36-component matrix into a single scalar for statistical purposes is presented. The third and final aim iss to demonstrate the value of both the stiffness matrix and its respective scalar by applying them experimentally to characterize the kinetics of a TDR. In particular, these metrics are used to evaluate the sagittal placement of the SYNTHES PRODISC-L TDR system and compare it to an intact vertebral disc. The results presented in this paper are the first such characterization of a TDR system.

An outline of the paper is as follows. In the following section, the parameterization of the displacement and relative rotation of a pair of vertebra is discussed. In the interests of conciseness, many of the details on the parameterization are placed in Appendix A. Section 2 contains a presentation of the stiffness matrix of a motion segment and a discussion of several of its unusual features. Most of the details on the derivation of this stiffness matrix are presented in Appendix B. A discussion of the kinetics of a motion segment follows. The application of the stiffness matrix K to the characterization of a TDR forms the primary focus of Section 3. In particular, the experimental measurements of K for an intact disc and three distinct placements of a TDR are presents. The paper closes with discussions of the objectives of the paper and how they were achieved, and the directions of future research on K. For the readers' convenience a section on nomenclature follows Section 4.

2 THEORY

A motion segment consists of two vertebral discs, an intervertebral disc, a pair of facet joints and the muscles and ligaments connecting the vertebra (cf. Fig. 1). The relative motion of the discs can be characterized by a set of three displacements and three Euler angles. The stiffness matrix K relates a set of forces and moments to the three displacements and three angles.

2.1 Kinematics

The three-dimensional displacement vector $\mathbf{y}$ is defined by the relative motion of two points X_1 and X_2, one on each vertebra. Although the selection of these points is arbitrary, their selection will effect the stiffness matrix. To define the Euler angles a pair of right-handed orthonormal bases is needed. One of these basis, which is denoted by $\{\mathbf{p}_1, \mathbf{p}_2, \mathbf{p}_3\}$ is fixed to the lower vertebra,

2. For further details on the necessities of using dual bases to describe moments and wrenches, the reader is referred to [23], [26], [27].

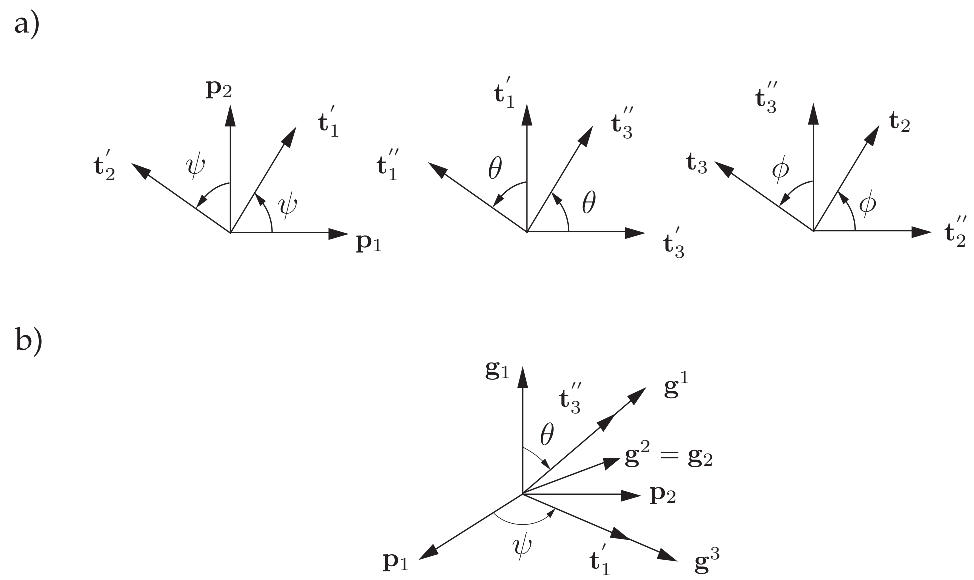

Fig. 2. *Schematic of the 3-2-1 set of Euler angles:* ψ, θ, *and* ϕ. *In this figure, the vectors* $\mathbf{g}_1 = \mathbf{p}_3$, $\mathbf{g}_2 = \mathbf{t}_2^{'} = \cos(\psi)\mathbf{p}_2 - \sin(\psi)\mathbf{p}_1$, *and* $\mathbf{g}_3 = \mathbf{t}_1^{''} = \cos(\theta)\mathbf{t}_1^{'} + \sin(\theta)\mathbf{p}_3$ *form the Euler basis. As illustrated in b), the dual Euler basis* $\{\mathbf{g}^1, \mathbf{g}^2, \mathbf{g}^3\}$ *is distinct from the Euler basis.*

and the other, which is denoted by $\{\mathbf{t}_1, \mathbf{t}_2, \mathbf{t}_3\}$ is affixed to the upper vertebra. An example featuring the L5/S1 motion segment is shown in Fig. 1.

In studies on the kinematics of the spine, it is standard to refer to the angles as axial rotation (ψ), lateral bending (θ), and flexion-extension (ϕ). Referring to Fig. 2(a), the axial rotation represents a rotation about $\mathbf{p}_3$ through an angle ψ. This is followed by a lateral bending about $\mathbf{t}_2^{'} = \cos(\psi)\,\mathbf{p}_1 + \sin(\psi)\,\mathbf{p}_2$. The final angle of rotation is a flexion-extension ϕ about $\mathbf{t}_1$. The axes of rotation $\mathbf{p}_3, \mathbf{t}_2^{'}$, and $\mathbf{t}_1$ define the Euler basis:

$$\begin{bmatrix} \mathbf{g}_1 \\ \mathbf{g}_2 \\ \mathbf{g}_3 \end{bmatrix} = \begin{bmatrix} \mathbf{p}_3 \\ \mathbf{t}_2^{'} \\ \mathbf{t}_1 \end{bmatrix} = \begin{bmatrix} 0 & 0 & 1 \\ -\sin(\psi) & \cos(\psi) & 0 \\ \cos(\theta)\cos(\psi) & \cos(\theta)\sin(\psi) & -\sin(\theta) \end{bmatrix} \begin{bmatrix} \mathbf{p}_1 \\ \mathbf{p}_2 \\ \mathbf{p}_3 \end{bmatrix}. \tag{1}$$

Based on the choice of axes, the set of Euler angles used here is known as the 3-2-1 set, and, as discussed by Crawford et al. [28], this is the optimal choice of Euler angles for the motion segment. Further details on the Euler angles used in this paper, the Euler basis and the dual Euler basis can be found in Appendix A.

2.2 The Stiffness Matrix K

To define the stiffness matrix K, one presumes that one can measure the resultant force and moment on one of the vertebra. For the upper vertebra, the resultant force is denoted by $\mathbf{F}_2$ and the resultant moment, relative to X_2, is denoted by $\mathbf{M}_2$. Correspondingly, the resultant force on the lower vertebra is denoted by $\mathbf{F}_1$ and the resultant moment, relative to X_1, is denoted by $\mathbf{M}_1$. When one measures these forces and moments and then correlates them to the displacements $\mathbf{y}$ and relative rotations ψ, θ, and ϕ, the forces and moments when the displacements and relative rotations are zero will not necessarily vanish. These residual forces and moments are denoted by a subscript 0. The stiffness matrix is then defined by the relationship

$$\mathsf{F} = \mathsf{F}_0 - \mathsf{K}\mathsf{d}. \tag{2}$$

In Eq. (2), the generalized force vector F, the generalized residual force vector F_0, the generalized displacement vector d, and stiffness matrix K are

$$\mathsf{F} = \begin{bmatrix} \mathbf{F}_2 \cdot \mathbf{p}_1 \\ \mathbf{F}_2 \cdot \mathbf{p}_2 \\ \mathbf{F}_2 \cdot \mathbf{p}_3 \\ \mathbf{M}_2 \cdot \mathbf{g}_1 \\ \mathbf{M}_2 \cdot \mathbf{g}_2 \\ \mathbf{M}_2 \cdot \mathbf{g}_3 \end{bmatrix}, \quad \mathsf{F}_0 = \begin{bmatrix} \mathbf{F}_{20} \cdot \mathbf{p}_1 \\ \mathbf{F}_{20} \cdot \mathbf{p}_2 \\ \mathbf{F}_{20} \cdot \mathbf{p}_3 \\ \mathbf{M}_{20} \cdot \mathbf{g}_1 \\ \mathbf{M}_{20} \cdot \mathbf{g}_2 \\ \mathbf{M}_{20} \cdot \mathbf{g}_3 \end{bmatrix}, \quad \mathsf{d} = \begin{bmatrix} \mathbf{y} \cdot \mathbf{p}_1 \\ \mathbf{y} \cdot \mathbf{p}_2 \\ \mathbf{y} \cdot \mathbf{p}_3 \\ \psi \\ \theta \\ \phi \end{bmatrix}, \quad \mathsf{K} = \begin{bmatrix} k_{11} & \cdots & k_{16} \\ \vdots & \ddots & \vdots \\ k_{61} & \cdots & k_{66} \end{bmatrix}. \tag{3}$$

The residual force $\mathbf{F}_{20}$ and residual moment $\mathbf{M}_{20}$ are the respective values of $\mathbf{F}_2$ and $\mathbf{M}_2$ when the displacement $\mathsf{d} = 0$.

There are several unusual features in Eq. (2). First, as shown in Eqs. (22) and (26) of Appendix B, the forces $\mathbf{F}_1$ and $\mathbf{F}_2$ are equal and opposite, as are the moments $\mathbf{M}_1$ and $\mathbf{M}_2$:

$$\mathbf{F}_1 = -\mathbf{F}_2, \qquad \mathbf{M}_1 = -\mathbf{M}_2. \tag{4}$$

Second, it is necessary to compute the components $\mathbf{M}_2 \cdot \mathbf{g}_k$, and as the Euler basis vectors $\mathbf{g}_k$ depend on the Euler angles θ and ψ these components are often not intuitive. Indeed, as discussed in the Appendix, computing $\mathbf{M}_2 \cdot \mathbf{g}_k$ is equivalent to expressing $\mathbf{M}_2$ in terms of it components relative to the dual Euler basis $\{\mathbf{g}^1, \mathbf{g}^2, \mathbf{g}^3\}$.[3]

In comparison to the stiffness matrix presented by Panjabi et al. [14], it is unrealistic to expect that K will be symmetric.[4] However, if attention is restricted to infinitesimal rotations, and the symmetry restrictions of Panjabi et al. are imposed, then K will simplify to the stiffness matrix proposed in [14].[5] The moment components determined by Panjabi et al.'s stiffness matrix correspond to $\mathbf{M} \cdot \mathbf{p}_k$. Unfortunately, it has long been known [23] that a constant moment $M_0\mathbf{p}_3$, where M_0 is a constant, is nonconservative when finite rotations are present. However, the moment $M_0\mathbf{g}^1$ is conservative. The use of the components $\mathbf{M}_2 \cdot \mathbf{g}_k$ in (3) are precisely to ensure that when K is symmetric, then $\mathbf{F}_2 - \mathbf{F}_{20}$ and $\mathbf{M}_2 - \mathbf{M}_{20}$ are guaranteed to be conservative even in the presence of finite rotations.

2.3 An Aggregate Stiffness Ratio

Comparison of the stiffness matrices for two motion segments on a term by term basis is difficult and often not very illuminating. An alternative strategy, which is proposed here, is to define a aggregate stiffness to be the norm of the stiffness matrix:

$$k = \sqrt{\mathrm{tr}\left(\mathsf{K}\mathsf{K}^T\right)}, \tag{5}$$

where tr denotes the trace of a matrix. To compare the aggregate stiffness of two motion segments, one can then define a normalized value S:

$$S = \frac{k_{\mathrm{I}} - k_{\mathrm{II}}}{k_{\mathrm{I}}}, \tag{6}$$

where k_{I} and k_{II} are the aggregate stiffnesses associated with the respective stiffness matrices of the two motion segments. The aggregate stiffness ratio S is distinct from the stability indices discussed in Howarth et al. [21]. Indeed, as one cannot expect the stiffness matrices to be symmetric or positive definite, such stability indices may not be revealing.

3. Details on the transformation of components of vectors relative to the bases used in this paper are summarized in Appendix C.

4. It is well-known in structural dynamics that the presence of nonconservative forces and moments can destroy the symmetry of the stiffness matrix.

5. The precise details on this equivalence can be found in Appendix B.1

3 Stiffness Alterations due to Total Disk Replacements

To demonstrate the utility of the stiffness matrix presented in this paper, the present section details its application to a data set that has recently been collected to determine the sensitivity of TDR placement along the saggital plane.

3.1 Experimental Protocol

Specimen Preparation

Healthy, non-degenerate fresh-frozen L5/S1 motion segments were harvested from human spines (n=5, mean age: 44, three females and two males). Specimen preparation included meticulous removal of muscular tissue so as to retain the integrity of the capsular and ligamentous elements. Afterwards, the specimens were potted in polymethylmetacrylate (PMMA), so that the S1 endplate was parallel to the PMMA surface and clamping faces.

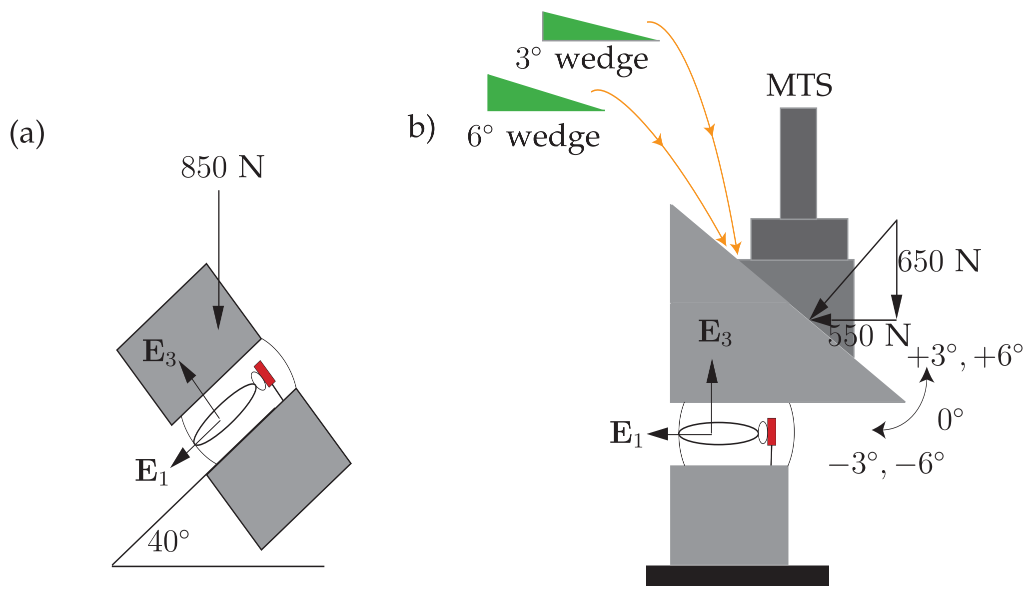

Fig. 3. *Schematic diagram of experimental set-up:* $40°$ *sacral slope and* 850 *N load in standing position: (a), Testing device constrained L5 posture in flexion, extension, and bending for investigating L5/S1 kinematics and (b), load is uniformly distributed and applies both shear of* 550 *N and compression of* 650 *N. In (b), the* $3°$ *and* $6°$ *wedges which are used to achieve the desired relative motion of the vertebrae are also shown.*

Mechanical Testing

Each specimen was placed in a servo-hydraulic apparatus (Bionix 858, MTS Systems Corp. Eden Meadow, MN) such that the disc was oriented at $40°$ relative to the horizontal axis (Fig. 3) as described previously in Rousseau et al. [12], [29]. The specimens were loaded with 850 N generating 650 N of disc compression and 550 N of horizontal shear consistent with free body analyses of L5/S1 based on specific morphometric studies.[6] Wedges were added at the frictionless interface to impose $3°$ and $6°$ of flexion, extension, and lateral bending postures, while axial torsion was unconstrained. The $12°$ total range of motion in the sagittal and the frontal plane was below the normal physiological zone of the L5/S1 joint [5].

Once tested with the disc intact, a TDR was performed (ProDisc-L, Synthes Inc. West Chester, PA USA). This particular device has a polyethylene (UHMWPE) on metal (CoCrMo) bearing

6. See, [19], [30]–[33].

interface with a non-retentive ball-and-socket design allowing 3 degrees-of-freedom. The device was initially positioned 3 mm (± 0.5 mm) posterior to the center of the inferior (S1) endplate. The specimen was tested in this position, and the device was then moved forward 3 mm to the central location and tested, followed by 3 mm anterior. This enabled measurement of the sensitivity of device placement along the sagittal plane.

Specimen preconditioning consisted of three cycles of complete loading and unloading prior to testing in each posture and was reduced to one cycle when the specimen was instrumented. During testing, data were collected after one minute of loading for each posture. Tissues were kept moist during testing by wrapping in saline-soaked gauze. A three-camera optoelectronic system (Motion Analysis Corpl, Santa Rosa, CA) was used to track the motion between the two vertebral bodies, while a load cell rigidly attached to S1 simultaneously recorded the resultant force and moments.

3.2 Data Analysis

Kinematic data was computed using software that integrated data from the load cell and motion analysis files. An optimization algorithm was applied to the optical targets between neutral (no wedge) and each of the rotated postures to get the optimal estimates of the Euler angles and the translation of a marker on L5 for each motion.[7] In this manner, the six components necessary to resolve the displacement vector d for each motion were determined.

Load cell data for each motion was translated into the six components of the generalized force vector F. The difference between rotated postures and the neutral posture were determined to give relative forces and moments. These vectors were then transformed to the dual Euler basis as described in the two earlier sections to allow accurate calculations despite the relatively large angles of rotation. The result is a six component vector $\mathsf{F} - \mathsf{F}_0$ consisting of three forces components and three moment components.

The displacement and load vectors for the rotations were organized into 6-by-6 matrices, d_E and F_E respectively, where each column represents a different motion, indicated by $m_1, \ldots, m_6$:

$$\mathsf{d}_E = \left[\ \{\mathsf{d}\}_{m_1} \quad \cdots \quad \{\mathsf{d}\}_{m_6}\ \right], \qquad \mathsf{F}_E = \left[\ \{\mathsf{F} - \mathsf{F}_0\}_{m_1} \quad \cdots \quad \{\mathsf{F} - \mathsf{F}_0\}_{m_6}\ \right]. \tag{7}$$

To compute the stiffness matrix K, one then computes $\mathsf{F}_E \left(\mathsf{d}_E\right)^{-1}$. The resulting matrix is composed of 36 stiffness coefficients relative to a neutral posture.

To analyze the TDRs influence on the stiffness matrix K of the motion segment, the stiffness matrix of the intact disc is compared to the corresponding matrix of the motion segment after the implantation of the TDR. The former and latter matrices are labeled by K_{I}, and K_{T}, respectively. Following Eq. (6), the stiffness ratio S was then computed:

$$S = \frac{k_{\mathrm{T}} - k_{\mathrm{I}}}{k_{\mathrm{I}}}, \tag{8}$$

where $k_{\mathrm{T,I}}$ are the aggregate stiffnesses associated with the matrices $\mathsf{K}_{\mathrm{T,I}}$.

3.3 Results

The four resultant stiffness matrices (intact and three device placements) varied considerably from specimen to specimen. In the interests of brevity, the outcomes are demonstrated with the stiffness matrices for a single representative specimen, and the aggregate stiffness ratio S is relied upon for interpreting general changes between device positions among the five motion segments.

7. The algorithm is based on the TRIAD algorithm and a classical optimal estimate of the translation. Discussions of these optimal estimates can be found in several papers, e.g., Dorst [34], Shuster and Oh [35], Spoor et al. [10], [36], and Woltring et al. [37].

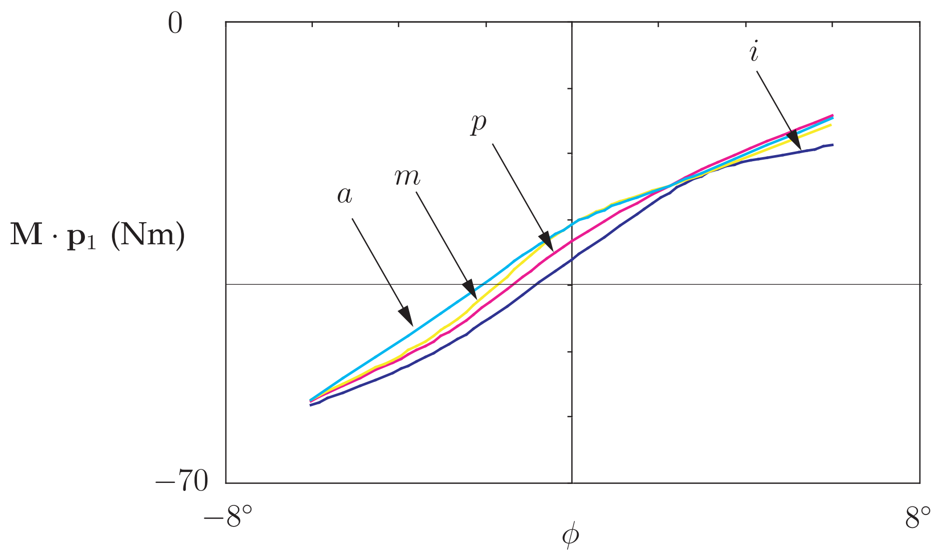

Fig. 4. *The moment component* $\mathbf{M}\cdot\mathbf{p}_1$ *as a function of the angle* ϕ *of flexion/extension for an intact motion segment and a three different positionings of a TDR. Here, and in Figs. 5 and 6, the label* i *stands for intact,* p *stands for posterior,* a *denotes anterior, and* m *denotes a centered positioning of the TDR.*

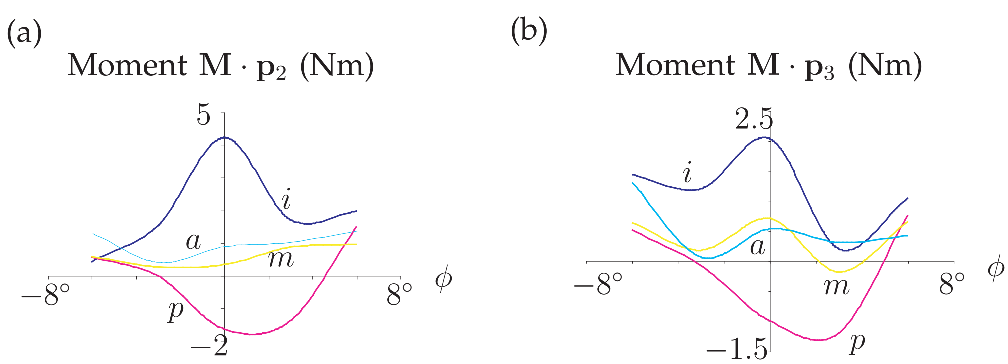

Fig. 5. *The moment components (a)* $\mathbf{M}\cdot\mathbf{p}_2$ *in the lateral direction and (b)* $\mathbf{M}\cdot\mathbf{p}_3$ *in the axial direction as a function of the angle* ϕ *of flexion/extension for an intact motion segment and a three different positionings of a TDR. The label* i *stands for intact,* p *stands for posterior,* a *denotes anterior, and* m *denotes a centered positioning of the TDR.*

3.3.1 Stiffness Matrices

For one of the five specimens, the following stiffness matrices were computed. The first of these matrices, K_i is for the intact specimens, while the matrices $\mathsf{K}_{p,m,a}$ correspond to the respective posterior, middle and anterior placements of the TDR:

$$\mathsf{K}_i = \begin{bmatrix} 80307 & 155477 & 29398 & -65.43 & -1102 & 1892.3 \\ 34377 & 382690 & 91836 & -113.8 & -1779 & 1585.5 \\ 8882.4 & -17381 & 3227.2 & -400 & -537.3 & 1630.6 \\ 599.5 & 1439.9 & 399.83 & -11.52 & -11.97 & 13.468 \\ 7544.9 & 16460 & 2832 & -50.85 & 174.02 & -276.9 \\ -105 & 7014.3 & 1468.5 & 7.9949 & -154.8 & 307.05 \end{bmatrix},$$

$$\mathsf{K}_p = \begin{bmatrix} 40731 & 31188 & 9704.2 & -315.8 & 35.422 & -393.2 \\ 59442 & 248555 & 52209 & -1510 & 1225 & -752.3 \\ 24364 & -46694 & 11257 & -977.4 & -1116 & 4754.9 \\ -74.46 & 560.93 & 66.933 & -1.935 & 8.0895 & -38.99 \\ -552.3 & -1369 & -53.01 & 107.87 & -81.85 & -454.9 \\ -5468 & -3523 & -973 & 97.05 & -23.56 & -234.9 \end{bmatrix},$$

$$\mathsf{K}_m = \begin{bmatrix} 36784 & 1954.5 & -8646 & 672.07 & 689.97 & -1651 \\ 39612 & 127890 & 62070 & -2068 & 4910.3 & -8295 \\ 4175.6 & 15301 & -6291 & 922.22 & -1258 & 2181.2 \\ 162.18 & 120.06 & 196.37 & -12.96 & 1.6026 & -12.87 \\ 6924.9 & 4106.4 & -623.5 & 107.96 & 49.332 & -147.8 \\ -2413 & 3323.1 & 547.01 & 28.409 & -153.3 & 227.34 \end{bmatrix},$$

$$\mathsf{K}_a = \begin{bmatrix} 18016 & 18719 & -8076 & 800.31 & -164.2 & -506 \\ -39459 & 186498 & 23518 & 1019.8 & -60.67 & -2705 \\ 22129 & -9158 & 1813.8 & -312.5 & 235.24 & 767.71 \\ 218.16 & 63.657 & 124.48 & -8.551 & -3.891 & 1.0397 \\ 4050.3 & 2576.9 & -1038 & 86.583 & -20.16 & -23.57 \\ -461.4 & -2808 & 574.83 & -70.38 & -8.937 & 103.03 \end{bmatrix}. \quad (9)$$

It is interesting to note that some of the diagonal stiffness elements are negative. In further contrast to the stiffness matrices reported in the literature, the matrices presented above are not symmetric. Concerning units, the displacements and rotations used to measure these matrices had units of meters and radians, respectively. Likewise, the forces and moments were computed using unit of Newtons and Newton meters. As a result, the stiffnesses have distinct units, for example, K_{11} has units of Newtons/meter, K_{16} and K_{61} have units of Newtons, and K_{45} has units of Newton meters.

3.3.2 Residual Forces and Moments and Negative Stiffnesses

The experimental set-up resulted in substantial moments of extension calculated about the center of the intact disc in the neutral position (see Fig. 4). This moment was calculated using the identity $\mathbf{M} = \mathbf{M}_{\mathrm{m}} + \boldsymbol{\pi} \times \mathbf{F}_{\mathrm{m}}$ where $\boldsymbol{\pi}$ is the position vector of the center of mass of the intact disc relative to the load cell and $\mathbf{F}_{\mathrm{m}}$ and $\mathbf{M}_{\mathrm{m}}$ are the force and moment measurements from the load cell. Furthermore, torsional and lateral bending moments were present during flexion and extension (see Fig. 5). Since the stiffness coefficients are calculated from the force and displacement vectors relative to the neutral posture, it is useful to display these results. It should be noticed from these figures that residual values of the moment $\mathbf{M}$ are present even when the angle $\phi = 0°$, and the slopes of these graphs are consistent with some of the negative values for individual stiffnesses that were found. In many cases, the motion segment had a more rigid response in the neutral posture than in the rotated postures, especially once the device was inserted. This can be explained by the high elastic modulus of the device which resists axial loads, but low coefficient of friction between the UHMWPE and the chrome-moly upon bending.

For each specimen, the aggregate stiffness ratio, S, between the instrumented and intact motion segment was calculated for the three device positions. The value of S is dimensionless and can be thought of as a fractional change from the intact disc. For instance, if the value of S is 0.5, the device caused the motion segment to respond 50% more rigidly than the intact disc on average over the six degrees-of-freedom. It was found that the average S of the five specimens that were tested was not significantly different ($P \leq 0.5$) for any of the device positions (Fig. 6), but there was a trend of increasing stiffness as the device was moved posteriorly.

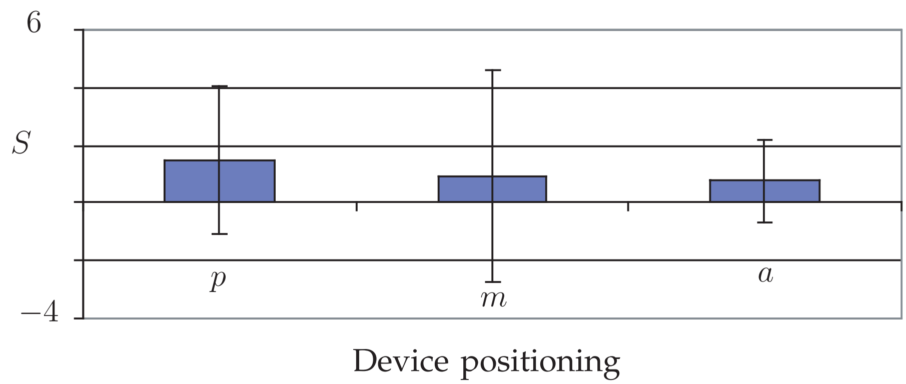

Fig. 6. *The values of the aggregate stiffness ratio S for various positionings of a TDR.*

4 Discussion

The objective of this paper was twofold. First, a new method of calculating the stiffness matrix that provides accurate calculations for large, more physiologic angles of rotation was described. This method is one of the only two possible formulations of this matrix which is valid for finite rotations.[8] The principal difference in the computation of the stiffness matrix for the finite rotation case compared to the classical counterpart is the need to use the values of the angles θ, ϕ, and ψ, when computing the moment components.

As a second objective, the stiffness matrix was used to compare the changes in kinetics induced by a TDR. Although several research efforts aimed at characterizing the kinematical changes induced by a TDR have appeared (see, e.g., [12], [29]), this paper has presented the the first kinetic comparison of a TDR to an intact disc. Three placements of the TDR were also considered in this comparison. In an attempt to distill the tremendous amount of data into a possibly clinically relevant metric, an aggregate stiffness ratio S was introduced. This ratio compares two matrices (in this case, instrumented versus intact) and distills the result into a single metric. Preliminary results of the S ratio calculations (cf. Fig. 6) display its ability as an efficient tool to compare and contrast devices as it is easy to interpret both clinically and statistically. There is a clear need for such a metric, apparent by the stream of technology that has poured into the orthopaedic spine community in the past decade. While further work is needed to prove its efficacy, its has the potential for quantifying device stiffness in vitro.

The stiffness matrix introduced in this paper is unique from those presented in earlier works since, as described above, the kinematic values are measured relative to a neutral or pre-loaded state. Additionally, previous studies in spinal kinetics have typically calculated each stiffness coefficient independently or assumed their value from symmetry. By combining six displacement vectors and their respective force vectors the stiffness matrix presented in this paper represents a comprehensive stiffness measure in all six degrees-of-freedom. Present work by the authors involves performing an extensive error analysis which aims to quantify how accurately one can determine the stiffness matrix K given the limitations inherent in the measurements of rotations, displacements, forces, and moments.

8. The second formulation, which would, in principle, feature screw theory and be based on the developments of Howard et al. [25] and Žefran and Kumar [26], remains to be fully developed.

ACKNOWLEDGMENTS

This material is based upon work supported by the National Science Foundation under Grant No. 0726675. Synthes Inc. is gratefully acknowledged for their financial support and donation of materials. Melodie Metzger and David Moody were supported by NSF graduate fellowships. The authors are grateful to Miguel Christophy for his assistance with Fig. 1 and to Nur Adila Faruk Senan for her help with the optimal estimation of the rigid body motion.

NOMENCLATURE

$\{\mathbf{p}_1, \mathbf{p}_2, \mathbf{p}_3\}$	$=$	right-handed orthonormal basis
$\{\mathbf{t}_1, \mathbf{t}_2, \mathbf{t}_3\}$	$=$	right-handed orthonormal basis
$\left\{\mathbf{t}_1^{'}, \mathbf{t}_2^{'}, \mathbf{t}_3^{'}\right\}$	$=$	right-handed orthonormal basis
$\left\{\mathbf{t}_1^{''}, \mathbf{t}_2^{''}, \mathbf{t}_3^{''}\right\}$	$=$	right-handed orthonormal basis
$\{\mathbf{g}_1, \mathbf{g}_2, \mathbf{g}_3\}$	$=$	Euler basis
$\left\{\mathbf{g}^1, \mathbf{g}^2, \mathbf{g}^3\right\}$	$=$	dual Euler basis
ψ, θ, ϕ	$=$	angles of axial rotation, lateral bending, and flexion-extension, respectively
$\boldsymbol{\omega}, \boldsymbol{\omega}_1, \boldsymbol{\omega}_2$	$=$	angular velocity vectors
$\mathbf{x}, \mathbf{x}_1, \mathbf{x}_2$	$=$	position vectors
$\mathbf{y} = \mathbf{x}_2 - \mathbf{x}_1$	$=$	displacement vector
R	$=$	rotation matrix
K	$=$	stiffness matrix of motion segment
K_{u}	$=$	stiffness matrix owing to conservative contributions
U	$=$	potential energy function
$\mathbf{F}_{\mathrm{c}_1}, \mathbf{F}_{\mathrm{c}_2}$	$=$	conservative forces
$\mathbf{M}_{\mathrm{c}_1}, \mathbf{M}_{\mathrm{c}_2}$	$=$	conservative moments
$\mathbf{F}_{\mathrm{m}}$	$=$	force measured by load cell
$\mathbf{M}_{\mathrm{m}}$	$=$	moment measured by load cell
$\mathbf{F}_{\mathrm{v}_1}, \mathbf{F}_{\mathrm{v}_2}$	$=$	viscoelastic forces
$\mathbf{M}_{\mathrm{v}_1}, \mathbf{M}_{\mathrm{v}_2}$	$=$	viscoelastic moments
$\mathbf{F}_{\mathrm{nc}_1}, \mathbf{F}_{\mathrm{nc}_2}$	$=$	nonconservative forces
$\mathbf{M}_{\mathrm{nc}_1}, \mathbf{M}_{\mathrm{nc}_2}$	$=$	nonconservative moments
F, F_0	$=$	generalized force vectors
d	$=$	generalized displacement vector
k	$=$	norm of the stiffness matrix
S	$=$	Aggregate stiffness ratio

APPENDIX A

BACKGROUND ON ROTATIONS, EULER ANGLES AND THE DUAL EULER BASIS

The rotation of interest is the relative rotation of a pair of vertebra $\mathcal{V}_1$ and $\mathcal{V}_2$. To parameterize the transformation induced by this rotation is a set of Euler angles is used. In this Appendix, relevant background on the Euler angles is presented which is based on the authorative review by Shuster [38] and supplemented by material on the dual Euler basis from [23], [27].

In what follows, it is presumed that a set of right-handed orthonormal basis vectors $\{\mathbf{p}_1, \mathbf{p}_2, \mathbf{p}_3\}$ are affixed to $\mathcal{V}_1$ and a similar set $\{\mathbf{t}_1, \mathbf{t}_2, \mathbf{t}_3\}$ are attached to $\mathcal{V}_2$ (see Fig. 1 and Fig. 7). The rotation of interest can be considered as transforming $\mathbf{p}_1$ to $\mathbf{t}_1$, $\mathbf{p}_2$ to $\mathbf{t}_2$, and $\mathbf{p}_3$ to $\mathbf{t}_3$.

As may be seen from Fig. 2(a), the manner in which the Euler angles parametrize the rotation is easily visualized by imagining two intermediate bases $\left\{\mathbf{t}_1^{'}, \mathbf{t}_2^{'}, \mathbf{t}_3^{'}\right\}$, $\left\{\mathbf{t}_1^{''}, \mathbf{t}_2^{''}, \mathbf{t}_3^{''}\right\}$. The first angle ψ represents the rotation of $\mathbf{p}_1$ and $\mathbf{p}_2$ about $\mathbf{p}_3$ to their respective transformed values $\mathbf{t}_1^{'}$ and $\mathbf{t}_2^{'}$. Similarly, the second rotation through the angle θ about the vector $\mathbf{t}_2^{'}$ and it transforms $\mathbf{t}_3^{'}$ and $\mathbf{t}_1^{'}$ into $\mathbf{t}_3^{''}$ and $\mathbf{t}_1^{''}$, respectively. The third rotation is through the angle ϕ about the vector $\mathbf{t}_1^{''}$. This final rotation transforms $\mathbf{t}_2^{''}$ and $\mathbf{t}_3^{''}$ into $\mathbf{t}_2$ and $\mathbf{t}_3$, respectively.

One can define a proper-orthogonal matrix R to represent the transformation of $\mathbf{p}_i$ to $\mathbf{t}_i$:

$$\begin{bmatrix} \mathbf{t}_1 \\ \mathbf{t}_2 \\ \mathbf{t}_3 \end{bmatrix} = \begin{bmatrix} R_{11} & R_{21} & R_{31} \\ R_{12} & R_{22} & R_{32} \\ R_{13} & R_{23} & R_{33} \end{bmatrix} \begin{bmatrix} \mathbf{p}_1 \\ \mathbf{p}_2 \\ \mathbf{p}_3 \end{bmatrix}, \qquad \begin{bmatrix} \mathbf{p}_1 \\ \mathbf{p}_2 \\ \mathbf{p}_3 \end{bmatrix} = \begin{bmatrix} R_{11} & R_{12} & R_{13} \\ R_{21} & R_{22} & R_{23} \\ R_{31} & R_{32} & R_{33} \end{bmatrix} \begin{bmatrix} \mathbf{t}_1 \\ \mathbf{t}_2 \\ \mathbf{t}_3 \end{bmatrix}, \tag{10}$$

where the components of the matrix are

$$\begin{bmatrix} R_{11} & R_{12} & R_{13} \\ R_{21} & R_{22} & R_{23} \\ R_{31} & R_{32} & R_{33} \end{bmatrix} = \begin{bmatrix} \mathrm{c}(\psi) & -\mathrm{s}(\psi) & 0 \\ \mathrm{s}(\psi) & \mathrm{c}(\psi) & 0 \\ 0 & 0 & 1 \end{bmatrix} \begin{bmatrix} \mathrm{c}(\theta) & 0 & \mathrm{s}(\theta) \\ 0 & 1 & 0 \\ -\mathrm{s}(\theta) & 0 & \mathrm{c}(\theta) \end{bmatrix} \begin{bmatrix} 1 & 0 & 0 \\ 0 & \mathrm{c}(\phi) & -\mathrm{s}(\phi) \\ 0 & \mathrm{s}(\phi) & \mathrm{c}(\phi) \end{bmatrix}. \tag{11}$$

Here, the abbreviations $\mathrm{c}(x)$ for $\cos(x)$ and $\mathrm{s}(x)$ for $\sin(x)$ have been used. The three axes of rotation for the individual angles associated with the set of Euler angles are known as the Euler basis vectors. These unit vectors are denoted by $\{\mathbf{g}_1, \mathbf{g}_2, \mathbf{g}_3\}$. For the 3-2-1 set of Euler angles, Eq. (1) provides a definition of $\{\mathbf{g}_1, \mathbf{g}_2, \mathbf{g}_3\}$ in terms of the basis vectors $\mathbf{p}_1, \mathbf{p}_2, \mathbf{p}_3$. Alternatively, with the help of Eq. (10) and Eq. (11), one can express the Euler basis vectors in terms of the basis vectors $\{\mathbf{t}_1, \mathbf{t}_2, \mathbf{t}_3\}$.

As can be verified from Eq. (1), the Euler basis vectors form a basis provided $\theta \neq \pm\frac{\pi}{2}$. As a result, one restricts the second angle $\theta \in \left(-\frac{\pi}{2}, \frac{\pi}{2}\right)$ to ensure that the Euler basis vectors form a basis. The angle θ measures lateral bending and so this restriction is trivially satisfied physiologically. The other two angles are free to range from 0 to 2π.

The angular velocity vector $\boldsymbol{\omega}$ associated with the rotation has a convenient representation when the Euler basis vectors are used:

$$\boldsymbol{\omega} = \dot{\psi}\mathbf{p}_3 + \dot{\theta}\mathbf{t}_2^{'} + \dot{\phi}\mathbf{t}_1. \tag{12}$$

In the sequel a set of vectors are need which can extract from $\boldsymbol{\omega}$ the angular speeds $\dot{\psi}$, $\dot{\theta}$, and $\dot{\phi}$. This set of vectors is known as the dual Euler basis vectors: $\{\mathbf{g}^1, \mathbf{g}^2, \mathbf{g}^3\}$.[9] By definition, the dual Euler basis vectors satisfy the relations

$$\boldsymbol{\omega} \cdot \mathbf{g}^1 = \dot{\psi}, \qquad \boldsymbol{\omega} \cdot \mathbf{g}^2 = \dot{\theta}, \qquad \boldsymbol{\omega} \cdot \mathbf{g}^3 = \dot{\phi}. \tag{13}$$

That is,

$$\begin{array}{lll} \mathbf{g}_1 \cdot \mathbf{g}^1 = 1, & \mathbf{g}_1 \cdot \mathbf{g}^2 = 0, & \mathbf{g}_1 \cdot \mathbf{g}^3 = 0, \\ \mathbf{g}_2 \cdot \mathbf{g}^1 = 0, & \mathbf{g}_2 \cdot \mathbf{g}^2 = 1, & \mathbf{g}_2 \cdot \mathbf{g}^3 = 0, \\ \mathbf{g}_3 \cdot \mathbf{g}^1 = 0, & \mathbf{g}_3 \cdot \mathbf{g}^2 = 0, & \mathbf{g}_3 \cdot \mathbf{g}^3 = 1. \end{array} \tag{14}$$

9. A thorough discussion of these basis vectors can be found in [23], [27].

Given the Euler basis vectors, one can use the nine equations Eq. (14) to compute expressions for the dual Euler basis vectors. After a series of straightforward manipulations, one would find that the dual Euler basis vectors have the representations

$$\begin{bmatrix} \mathbf{g}^1 \\ \mathbf{g}^2 \\ \mathbf{g}^3 \end{bmatrix} = \begin{bmatrix} \cos(\psi)\tan(\theta) & \sin(\psi)\tan(\theta) & 1 \\ -\sin(\psi) & \cos(\psi) & 0 \\ \cos(\psi)\sec(\theta) & \sin(\psi)\sec(\theta) & 0 \end{bmatrix} \begin{bmatrix} \mathbf{p}_1 \\ \mathbf{p}_2 \\ \mathbf{p}_3 \end{bmatrix}. \tag{15}$$

It is important to note that the vectors $\mathbf{g}^1$ and $\mathbf{g}^3$ do not have unit magnitude (cf. Fig. 2(b)). Expressions for the dual Euler basis vectors in terms of $\{\mathbf{t}_1, \mathbf{t}_2, \mathbf{t}_3\}$ can established using Eq. (11) and Eq. (15)

If the Euler angles are infinitesimal, then, from Eq. (15), it is easy to see that

$$\mathbf{g}^1 \approx \mathbf{p}_3 \approx \mathbf{t}_3, \qquad \mathbf{g}^2 \approx \mathbf{p}_2 \approx \mathbf{t}_2, \qquad \mathbf{g}^3 \approx \mathbf{p}_1 \approx \mathbf{t}_1. \tag{16}$$

Related results hold for the Euler basis vectors $\mathbf{g}_k$. For the spinal applications of interest, the angles of rotation are not infinitesimal and so the approximations Eq. (16) cannot be used.

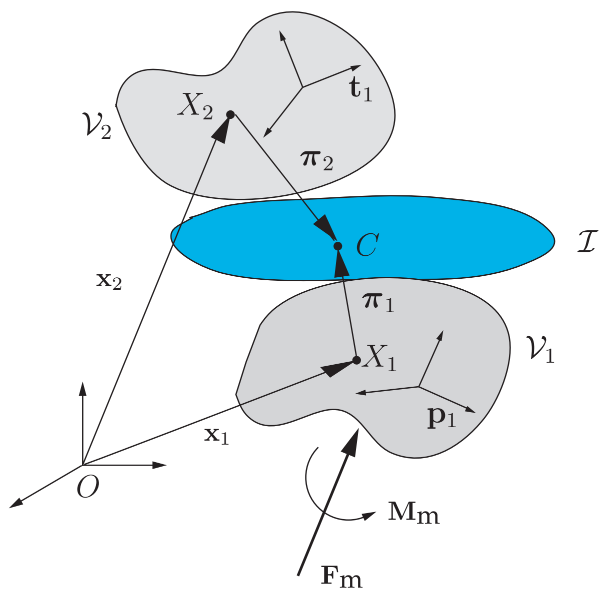

Fig. 7. A schematic drawing of an intervebral disc $\mathcal{I}$ between the vertebra $\mathcal{V}_1$ and $\mathcal{V}_2$. The point C of the disc $\mathcal{I}$ has a position vector $\mathbf{x}_1 + \boldsymbol{\pi}_1 = \mathbf{x}_2 + \boldsymbol{\pi}_2$ relative to the fixed origin O. The force $\mathbf{F}_{\mathrm{m}}$ and moment $\mathbf{M}_{\mathrm{m}}$ shown in this figure are supplied by the load cell.
fig:vertunit

Appendix B
Derivation of the Stiffness Matrix of a Motion Segment

Consider the system consisting of two vertebra $\mathcal{V}_1$ and $\mathcal{V}_2$ located on either side of an intervertebral disc $\mathcal{I}$ shown in Fig. 7. Of interest in this paper is the development of a mechanical model for the intervertebral disc and the facet joints. It is assumed that the disc and joints result in a force $\mathbf{F}_1$ and a moment $\mathbf{M}_1$ on $\mathcal{V}_1$ and a force $\mathbf{F}_2$ and a moment $\mathbf{M}_2$ on $\mathcal{V}_2$. The force $\mathbf{F}_1$ is assumed to act at the material point X_1 of $\mathcal{V}_1$ and the moment $\mathbf{M}_1$ is taken relative to this point (cf. Fig. 1). Similarly, $\mathbf{F}_2$ is assumed to act at the material point X_2 of $\mathcal{V}_2$ and the moment $\mathbf{M}_2$ is relative to X_2. In an experimental apparatus to examine the kinetics of a segment of the spine, it is standard to place a load cell directly under the vertebral body $\mathcal{V}_1$. The load cell provides two sets of measurements: the three force components and three moment components: $\mathbf{F}_{\mathrm{m}_k} = \mathbf{F}_{\mathrm{m}} \cdot \mathbf{p}_k$ and $\mathbf{M}_{\mathrm{m}_k} = \mathbf{M}_{\mathrm{m}} \cdot \mathbf{p}_k$ where $k = 1, 2, 3$.

The rotation of $\mathcal{V}_2$ relative to $\mathcal{V}_1$ can be characterized by a rotation R. The rotation is parameterized in this paper using a set of a set of 3-2-1 Euler angles: ψ, θ, and ϕ. Hence, the difference between the angular velocity vectors $\boldsymbol{\omega}_1$ and $\boldsymbol{\omega}_2$ of $\mathcal{V}_1$ and $\mathcal{V}_2$ can be expressed as[10]

$$\boldsymbol{\omega}_2 - \boldsymbol{\omega}_1 = \dot{\psi}\mathbf{g}_1 + \dot{\theta}\mathbf{g}_2 + \dot{\phi}\mathbf{g}_3. \tag{17}$$

The position vectors of the points X_1 and X_2 of the vertebrae are denoted by $\mathbf{x}_1$ and $\mathbf{x}_2$, respectively. It is standard to express these vectors in terms of the fixed basis $\{\mathbf{p}_1, \mathbf{p}_2, \mathbf{p}_3\}$, e.g., $\bar{\mathbf{x}}_1 = \sum_{k=1}^{3} x_{1_k}\mathbf{p}_k$. Furthermore, it is necessary to define the relative displacement vector of the point X_2 relative to X_1:

$$\mathbf{y} = y_1\mathbf{p}_1 + y_2\mathbf{p}_2 + y_3\mathbf{p}_3 = \mathbf{x}_2 - \mathbf{x}_1. \tag{18}$$

Although, it is customary to choose X_1 to be the center of mass of $\mathcal{V}_1$ and X_2 to be the center of mass of $\mathcal{V}_2$, this choice is often not convenient. Further, precise identification of the center of mass of a vertebra is non-trivial.

B.1 Potential Energy, Conservative Forces, and Conservative Moments

To postulate a potential energy for the motion segment and correlate its derivatives to the forces and moments on the vertebra, the methodology used in O'Reilly and Srinivasa [24] is followed.[11] The crucial assumption is that the potential energy for the conservative forces and conservative moments supplied by the facets, ligaments, and intervertebral disc is

$$U = U(\mathbf{y}, \psi, \theta, \phi). \tag{19}$$

In this case, the relative translation and rotation of the vertebra are independent. The forces ($\mathbf{F}_{\mathrm{C}_1}$ and $\mathbf{F}_{\mathrm{C}_2}$) and moments ($\mathbf{M}_{\mathrm{C}_1}$ and $\mathbf{M}_{\mathrm{C}_2}$) supplied by the disc, facets, and ligaments to the vertebrae are conservative:[12]

$$-\dot{U} = \mathbf{F}_{\mathrm{C}_1} \cdot \dot{\mathbf{x}}_1 + \mathbf{F}_{\mathrm{C}_2} \cdot \dot{\mathbf{x}}_2 + \mathbf{M}_{\mathrm{C}_1} \cdot \boldsymbol{\omega}_1 + \mathbf{M}_{\mathrm{C}_2} \cdot \boldsymbol{\omega}_2. \tag{20}$$

As

$$\dot{U} = \sum_{i=1}^{3} \frac{\partial U}{\partial y_i}\dot{y}_i + \frac{\partial U}{\partial \psi}\dot{\psi} + \frac{\partial U}{\partial \theta}\dot{\theta} + \frac{\partial U}{\partial \phi}\dot{\phi}, \tag{21}$$

it can be concluded that

$$\begin{aligned} \mathbf{F}_{\mathrm{C}_1} = -\mathbf{F}_{\mathrm{C}_2} &= \sum_{i=1}^{3} \frac{\partial U}{\partial y_i}\mathbf{p}_i, \\ \mathbf{M}_{\mathrm{C}_1} = -\mathbf{M}_{\mathrm{C}_2} &= \frac{\partial U}{\partial \psi}\mathbf{g}^1 + \frac{\partial U}{\partial \theta}\mathbf{g}^2 + \frac{\partial U}{\partial \phi}\mathbf{g}^3. \end{aligned} \tag{22}$$

These are the conservative forces and moments exerted by the disc on the vertebrae. The simplicity of the representations for the conservative moments $\mathbf{M}_{\mathrm{C}_1}$ and $\mathbf{M}_{\mathrm{C}_2}$ is directly attributable to the use of the dual Euler basis.

10. The interested reader is referred to Casey and Lam [39] where a discussion of relative angular velocity vectors can be found.

11. Their work is compatible with, and a generalization of, works on moment potentials (e.g., [40], [41]) and is entirely consistent with previous developments on moment potentials in the dynamics of rigid bodies.

12. In [24], X_1 and X_2 are chosen to be the centers of mass. A comparison of the expressions for the resultant moment relative to a center of mass and an arbitrary material point can be used to show that this restriction can be removed, and it is done so here without further comment.

Assuming that U is a quadratic function of $\mathbf{y}$ and the Euler angles, a Taylor series expansion would show that

$$\begin{aligned} U \;=\; & \frac{1}{2}\begin{bmatrix} y_1 & y_2 & y_3 \end{bmatrix}\begin{bmatrix} a_{11} & a_{12} & a_{13} \\ a_{12} & a_{22} & a_{23} \\ a_{13} & a_{23} & a_{33} \end{bmatrix}\begin{bmatrix} y_1 \\ y_2 \\ y_3 \end{bmatrix} + \begin{bmatrix} y_1 & y_2 & y_3 \end{bmatrix}\begin{bmatrix} b_{11} & b_{12} & b_{13} \\ b_{21} & b_{22} & b_{23} \\ b_{31} & b_{32} & b_{33} \end{bmatrix}\begin{bmatrix} \psi \\ \theta \\ \phi \end{bmatrix} \\ & +\frac{1}{2}\begin{bmatrix} \psi & \theta & \phi \end{bmatrix}\begin{bmatrix} c_{11} & c_{12} & c_{13} \\ c_{12} & c_{22} & c_{23} \\ c_{13} & c_{23} & c_{33} \end{bmatrix}\begin{bmatrix} \psi \\ \theta \\ \phi \end{bmatrix}. \end{aligned} \tag{23}$$

This function has 21 unknown coefficients. Examples featuring the identification of these coefficients occupies Section 3.2 of the present paper.

One can view the potential energy function U as a generalization of a potential energy function for a motion segment that was proposed by Panjabi et al. [14]. Their function assumed infinitesimal rotations and was intended for use in the thoracic region of the spine. The value of present formulation is that one no longer needs to impose such kinematic restrictions. The added expense, however, is that one needs to keep track of the Euler angles during measurements of forces and moments. If one restricts attention to infinitesimal rotations, then the expressions for $\mathbf{g}^i$ simplify (cf. Eq. (16)). If one then imposes the symmetry restrictions used in [14], then the U presented in Eq. (23) would reduce to the function proposed by Panjabi, Brand and White with its 12 coefficients.

To facilitate further comparison to the Panjabi, Brand and White function, one can compute, with the help of Eq. (22) and Eq. (23), the relationship between the conservative forces and conservative moments and the translational and angular displacements. These results are expressed in the compact form:

$$\mathsf{F_C} = -\mathsf{K_U}\mathsf{d}, \tag{24}$$

where the generalized force vector $\mathsf{F_C}$, generalized displacement vector d, and stiffness matrix $\mathsf{K_U}$ are

$$\mathsf{F_C} = \begin{bmatrix} \mathbf{F}_{\mathrm{C}_2}\cdot\mathbf{p}_1 \\ \mathbf{F}_{\mathrm{C}_2}\cdot\mathbf{p}_2 \\ \mathbf{F}_{\mathrm{C}_2}\cdot\mathbf{p}_3 \\ \mathbf{M}_{\mathrm{C}_2}\cdot\mathbf{g}_1 \\ \mathbf{M}_{\mathrm{C}_2}\cdot\mathbf{g}_2 \\ \mathbf{M}_{\mathrm{C}_2}\cdot\mathbf{g}_3 \end{bmatrix}, \qquad \mathsf{d} = \begin{bmatrix} y_1 \\ y_2 \\ y_3 \\ \psi \\ \theta \\ \phi \end{bmatrix}, \qquad \mathsf{K_U} = \begin{bmatrix} a_{11} & a_{12} & a_{13} & b_{11} & b_{12} & b_{13} \\ a_{12} & a_{22} & a_{23} & b_{21} & b_{22} & b_{23} \\ a_{13} & a_{23} & a_{33} & b_{31} & b_{32} & b_{33} \\ b_{11} & b_{21} & b_{31} & c_{11} & c_{12} & c_{13} \\ b_{12} & b_{22} & b_{32} & c_{12} & c_{22} & c_{23} \\ b_{13} & b_{23} & b_{33} & c_{13} & c_{23} & c_{33} \end{bmatrix}. \tag{25}$$

The corresponding forces $\mathbf{F}_{\mathrm{C}_1}$ and moments $\mathbf{M}_{\mathrm{C}_1}$ on $\mathcal{V}_1$ are equal and opposite to $\mathbf{F}_{\mathrm{C}_2}$ and $\mathbf{M}_{\mathrm{C}_2}$, respectively (cf. Eq. (22)). It needs to be emphasized that the components of the moments in Eq. (24) are taken relative to the Euler basis: $\mathbf{M}_{\mathrm{C}_2} = -\mathbf{M}_{\mathrm{C}_1} = \sum_{k=1}^{3}\left(\mathbf{M}_{\mathrm{C}_2}\cdot\mathbf{g}_k\right)\mathbf{g}^k$.

B.2 Viscous Forces and Viscous Moments

It is well-known that the intervertebral disc is a viscoelastic body and consequently any model for the motion segment must accommodate this behavior. Here, the simplest possible viscous terms are considered and it is assumed that the viscoelastic forces ($\mathbf{F}_{\mathrm{V}_1}$ and $\mathbf{F}_{\mathrm{V}_2}$) and moments ($\mathbf{M}_{\mathrm{V}_1}$ and $\mathbf{M}_{\mathrm{V}_2}$) have the representations

$$\begin{aligned} \mathbf{F}_{\mathrm{V}_2} = -\mathbf{F}_{\mathrm{V}_1} \;&=\; -c_1\dot{y}_1\mathbf{p}_1 - c_2\dot{y}_2\mathbf{p}_2 - c_3\dot{y}_3\mathbf{p}_3, \\ \mathbf{M}_{\mathrm{V}_2} = -\mathbf{M}_{\mathrm{V}_1} \;&=\; -d_1\dot{\psi}\mathbf{g}^1 - d_2\dot{\theta}\mathbf{g}^2 - d_3\dot{\phi}\mathbf{g}^3. \end{aligned} \tag{26}$$

It is easy to motivate the assumption that the constants d_k and c_k are non-negative by examining the combined power $\mathcal{P}$ of these forces and moments:[13]

$$\begin{aligned}\mathcal{P} &= \sum_{i=1}^{2} \left(\mathbf{F}_{\mathrm{V}_i} \cdot \dot{\mathbf{x}}_i + \mathbf{M}_{\mathrm{V}_i} \cdot \boldsymbol{\omega}_i\right) \\ &= -\left(\sum_{k=1}^{3} c_k \dot{y}_k \dot{y}_k\right) - d_1\dot{\psi}^2 - d_2\dot{\theta}^2 - d_3\dot{\phi}^2. \end{aligned} \tag{27}$$

Clearly, $\mathcal{P} \leq 0$ if $d_k \geq 0$ and $c_k \geq 0$. More complex forms of the forces and moments shown in Eq. (26) are eminently possible, but these suffice for the present purposes. It is also important to note that even if the d_k's had equal value, neither $\mathbf{M}_{\mathrm{V}_2}$ nor $\mathbf{M}_{\mathrm{V}_1}$ are necessarily parallel to $\boldsymbol{\omega}_2 - \boldsymbol{\omega}_1$. The viscous and conservative components of the forces and moments can be additively combined to obtain the viscoelastic forces due to the vertebral joint: e.g., $\mathbf{F}_1 = \mathbf{F}_{\mathrm{C}_1} + \mathbf{F}_{\mathrm{V}_1}$.

B.3 Nonconservative Contributions

In addition to the aforementioned viscoelastic contributions, the resultant forces and moments experienced by the vertebra will also include nonconservative contributions due to the contact forces in the facet joints and activation forces in the ligaments. Labelling these nonconservative contributions with the subscript nc, one has the following expressions for the resultant forces and moments:

$$\mathbf{F}_k = \mathbf{F}_{\mathrm{nc}_k} + \mathbf{F}_{\mathrm{C}_k} + \mathbf{F}_{\mathrm{V}_k}, \quad \mathbf{M}_k = \mathbf{M}_{\mathrm{nc}_k} + \mathbf{M}_{\mathrm{C}_k} + \mathbf{M}_{\mathrm{V}_k}, \tag{28}$$

where $k = 1, 2$. As with the previous developments $\mathbf{F}_1 = -\mathbf{F}_2$ and $\mathbf{M}_1 = -\mathbf{M}_2$.

B.4 The Stiffness Matrix of the Vertebral Unit

To accommodate these residual forces and moments, one performs a Taylor series expansion of the forces $\mathbf{F}_1$ and $\mathbf{F}_2$ and moments $\mathbf{M}_1$ and $\mathbf{M}_2$. Truncating this expansion at second order, ignoring the viscous contribution, leads to a representation of the form shown in Eq. (2) for $\mathbf{F}_2$ and $\mathbf{M}_2$

APPENDIX C
TRANSFORMING MOMENTS

It is often desired to transform the components of a vector with respect to the basis $\{\mathbf{p}_1, \mathbf{p}_2, \mathbf{p}_3\}$ to the corresponding components with respect to the bases $\{\mathbf{g}^1, \mathbf{g}^2, \mathbf{g}^3\}$ and $\{\mathbf{t}_1, \mathbf{t}_2, \mathbf{t}_3\}$. Denoting this vector by $\mathbf{b}$, the following representations of this vector can be defined:

$$\mathbf{b} = \sum_{k=1}^{3} B_k \mathbf{p}_k = \sum_{k=1}^{3} b_k \mathbf{t}_k = \sum_{k=1}^{3} \beta_k \mathbf{g}^k. \tag{29}$$

Then, with the help of Eqs. (1), (10), and (15), one finds that

$$\begin{aligned}\begin{bmatrix} b_1 \\ b_2 \\ b_3 \end{bmatrix} &= \begin{bmatrix} R_{11} & R_{21} & R_{31} \\ R_{12} & R_{22} & R_{32} \\ R_{13} & R_{23} & R_{33} \end{bmatrix} \begin{bmatrix} B_1 \\ B_2 \\ B_3 \end{bmatrix}, \\ \begin{bmatrix} \beta_1 \\ \beta_2 \\ \beta_3 \end{bmatrix} &= \begin{bmatrix} 0 & 0 & 1 \\ -\sin(\psi) & \cos(\psi) & 0 \\ \cos(\theta)\cos(\psi) & \cos(\theta)\sin(\psi) & -\sin(\theta) \end{bmatrix} \begin{bmatrix} B_1 \\ B_2 \\ B_3 \end{bmatrix}. \end{aligned} \tag{30}$$

In the interests of brevity, the reader is referred to Eq. (11) where expressions for the components R_{ik} can be found.

13. This calculation is facilitated by the fact that the dual Euler basis was used to establish representations for $\mathbf{M}_{\mathrm{V}_1}$ and $\mathbf{M}_{\mathrm{V}_2}$.

References

[1] R. Bertagnoli and S. Kumar, "Indications for full prosthetic disc arthroplasty: A correlation of clinical outcomes against a variety of indications," *Eur. Spine J.*, vol. 11, no. Supplement No. 2, pp. S131–S136, 2002.

[2] B. W. Cunningham, A. E. Dmitriev, N. Hu, and P. C. McAfee, "General principles of total disc replacement arthroplasty: Seventeen cases in a nonhuman primate model," *Spine*, vol. 28, pp. S118–S124, 2004.

[3] M. de Kleuver, F. C. Oner, and W. C. Jacobs, "Total disc replacement for chronic low back pain: Background and a systematic review of the literature," *Eur. Spine J.*, vol. 12, no. 2, pp. 108–116, 2003.

[4] I. M. Punt, V. M. Visser, L. W. van Rhijn, S. M. Kurtz, J. Antonis, G. W. H. Schurink, and A. van Ooij, "Complications and reoperations of the SB Charité lumbar disc prosthesis: Experience in 75 patients," *Eur. Spine J.*, vol. 17, no. 1, pp. 36–43, 2008.

[5] M. M. Panjabi, T. Oxland, I. Yamamoto, and J. Crisco, "Mechanical behavior of the human lumbar and lumbosacral spine shown by three-dimensional load displacement curves," *J. Bone Joint Surg. Am.*, vol. 76, no. 3, pp. 413–424, 1994.

[6] T. G. Mayer, G. Kondraske, S. B. Beals, and R. J. Gatchel, "Spinal range of motion. Accuracy and sources of error with inclinometric measurement," *Spine*, vol. 22, no. 17, pp. 1976–1984, 1997.

[7] B. W. Cunningham, Y. Kotani, P. S. McNulty, A. Cappuccino, and P. C. McAfee, "The effect of spinal destabilization and instrumentation on lumbar intradiscal pressure: An in vitro biomechanical analysis," *Spine*, vol. 22, no. 22, pp. 2655–2663, 1997.

[8] M. M. Panjabi, "The stabilizing system of the spine. Part II. Neutral zone and instability hypothesis," *J. Spinal Disorders*, vol. 5, no. 4, pp. 390–397, 1992.

[9] M. Mansour, S. Spiering, C. Lee, H. Dathe, A. K. Kalscheuer, D. Kubein-Meesenburg, and H. Nägerl, "Evidence for iha migration during axial rotation of a lumbar spine segment by using a novel high-resolution 6d kinematic tracking system," *J. Biomech.*, vol. 37, 2004.

[10] C. Spoor, "Explanation, verification and application of helical-axis error propogation formulae," *Human Movement Science*, vol. 3, no. 1–2, pp. 95–117, 1984.

[11] D. S. Adams. M. A., McNally and P. Dolan, "'stress' distributions inside intervertebral discs: The effects of age and degeneration," *J. Bone Joint Surg. Am.*, vol. 78, no. 6, pp. 965–972, 1996.

[12] M. A. Rousseau, D. S. Bradford, R. Bertagnoli, S. S. Hu, and J. C. Lotz, "Disc arthroplasty design influences intervertebral kinematics and facet forces," *The Spine Journal*, vol. 6, no. 3, pp. 258–266, 2006.

[13] M. Sharma, N. A. Langrana, and J. Rodriguez, "Role of ligaments and facets in lumbar spinal stability," *Spine*, vol. 20, no. 8, pp. 887–900, 1995.

[14] M. M. Panjabi, R. A. Brand Jr., and A. A. White, "Three-dimensional flexibility and stiffness properties of the human thoracic spine," *J. Biomech.*, vol. 9, no. 4, pp. 185–192, 1976.

[15] M. G. Gardner-Morse and I. A. Stokes, "Physiological axial compressive preloads increase motion segment stiffness, linearity and hysteresis in all six degrees of freedom for small displacements about the neutral posture," *J. Orthop. Res.*, vol. 21, no. 3, pp. 547–552, 2003.

[16] M. G. Gardner-Morse and I. A. F. Stokes, "Structural behavior of the human lumbar spinal motion segments," *J. Biomech.*, vol. 37, no. 2, pp. 205–212, 2004.

[17] I. A. Stokes, M. G. Gardner-Morse, D. Churchill, and J. P. Laible, "Measurement of a spinal motion segment stiffness matrix," *J. Biomech.*, vol. 35, no. 4, pp. 517–521, 2002.

[18] I. A. F. Stokes and J. C. Iatridis, *Basic Orthopaedic Biomechanics and Mechano-Biology*, 3rd ed. Philadelphia: Lippincott Williams & Wilkins, 2005, ch. Biomechanics of the Spine, pp. 529–561, Edited by V. C. Mow and R. Huiskes.

[19] S. McGill and R. Norman, "Effects of an anatomically detailed erector spinae model on L4/L5 disc compression and shear," *J. Biomech.*, vol. 20, no. 6, pp. 591–600, 1987.

[20] J. Cholewicki and S. M. McGill, "Mechanical stability of the in vivo lumbar spine: Implications for injury and chronic low back pain," *Clin. Biomech.*, vol. 11, no. 1, pp. 1–15, 1996.

[21] S. J. Howarth, A. E. Allison, S. G. Grenier, J. Cholewicki, and S. M. McGill, "On the implications of interpreting the stability index: A spine example," *J. Biomech.*, vol. 37, no. 8, pp. 1147–1154, 2004.

[22] S. M. McGill, S. J., and G. Bennett, "Passive stiffness of the lumbar torso about the flexion-extension, lateral bend and axial twist axes: The effect of belt wearing and breath holding." *Spine*, vol. 19, no. 6, pp. 696–704, 1994.

[23] O. M. O'Reilly, "The dual Euler basis: Constraints, potential energies and Lagrange's equations in rigid body dynamics," *J. Appl. Mech.*, vol. 74, no. 2, pp. 256–258, 2007.

[24] O. M. O'Reilly and A. R. Srinivasa, "On potential energies and constraints in the dynamics of rigid bodies and particles," *Math. Probl. Eng.*, vol. 8, no. 3, pp. 169–180, 2002.

[25] S. Howard, M. Žefran, and V. Kumar, "On the 6×6 Cartesian stiffness matrix for three-dimensional motions," *Mech. Mach. Theory*, vol. 33, no. 4, pp. 389–408, 1998.

[26] M. Žefran and V. Kumar, "A geometrical approach to the study of the Cartesian stiffness matrix," *J. Mech. Design*, vol. 124, no. 1, pp. 30–38, 2002.

[27] O. M. O'Reilly, *Intermediate Engineering Dynamics: A Unified Approach to Newton-Euler and Lagrangian Mechanics*. New York: Cambridge University Press, 2008.

[28] N. R. Crawford, G. T. Yamaguchi, and C. A. Dickman, "Methods for determining spinal flexion/extension, lateral bending, and axial rotation from marker coordinate data: Analysis and refinement," *Human Movement Science*, vol. 15, no. 1, pp. 55–78, 1996.

[29] M. A. Rousseau, D. S. Bradford, T. M. Hadi, K. L. Pedersen, and J. C. Lotz, "The instant axis of rotation influences facet forces at L5/S1 during flexion/extension and lateral bending," *Eur Spine J.*, vol. 15, no. 3, pp. 299–307, 2006.

[30] M. Adams, W. Hutton, and J. Stott, “The resistance to flexion of the lumbar intervertebral joint,” *Spine*, vol. 5, pp. 245–253, 1980.
[31] G. Duval-Beaupere and G. Robain, “Visualization on full spine radiographs of the anatomical connections of the centers of the segmental body mass supported by each vertebra and measured in vivo,” *Int. Orthop.*, vol. 11, pp. 261–269, 1987.
[32] K. McGlashen, J. Miller, A. Schultz, and G. Andersson, “Load displacement behavior of the human lumbo-sacral joint,” *J. Orthop. Res.*, vol. 5, no. 4, pp. 488–496, 1987.
[33] A. A. White III and M. M. Panjabi, *Clinical Biomechanics of the Spine*, 2nd ed. Philadelphia: Lippincott Williams & Wilkins, 1990.
[34] L. Dorst, “First order error propagation of the Procrustes method for 3D attitude estimation,” *IEEE T. Pattern Anal.*, vol. 27, no. 2, pp. 221–229, 2005.
[35] M. D. Shuster and S. D. Oh, “Three-axis attitude determination from vector observations,” *J. Guidance*, vol. 4, no. 1, pp. 70–77, 1981.
[36] C. W. Spoor and F. E. Veldpaus, “Rigid body motion calculated from spatial co-ordinates of markers,” *J. Biomech.*, vol. 13, no. 4, pp. 391–393, 1980.
[37] H. J. Woltring, R. Huiskes, A. de Lange, and F. E. Veldpaus, “Finite centroid and helical axis estimation from noisy landmark measurements in the study of human joint kinematics,” *J. Biomech.*, vol. 18, no. 5, pp. 379–389, 1985.
[38] M. D. Shuster, “A survey of attitude representations,” *J. Astronaut. Sci.*, vol. 41, no. 4, pp. 439–517, 1993.
[39] J. Casey and V. C. Lam, “On the relative angular velocity tensor,” *ASME J. Mech. Transm.*, vol. 108, pp. 399–400, 1986.
[40] S. S. Antman, “Solution to Problem 71–24: ”Angular velocity and moment potentials for a rigid body,” by J. G. Simmonds,” *SIAM Review*, vol. 14, pp. 649–652, 1972.
[41] J. G. Simmonds, “Moment potentials,” *Am. J. Phys.*, vol. 52, no. 9, pp. 851–852, 1984, errata published on page 277 of Vol. 53.